SUSPENDED SEDIMENT TRANSPORT INSIDE AND OUTSIDE SURF ZONES

Andres Payo[1], Nobuhisa Kobayashi[2], Fumihiko Yamada[3],

Juan J. Muñoz-Pérez[4]

Velocities and sand concentrations measured along 20 transects at the Field Research Facility (FRF) at Duck, North Carolina during October 16–23, 1997 are analyzed to examine the cross-shore and longshore suspended sand transport in the FRF pier depression. The suspended sand volume per unit bottom area remains large outside the surf zone in the depression. The depth integrated offshore and longshore suspended sand transport rates are shown to be proportional to the products of the suspended sand volume and the depth-averaged cross-shore and longshore currents. The offshore suspended sand transport rate at the end of the pier is estimated to be as large as 3.5 m^3/hr/m at the peak of a storm with an offshore significant wave height of 3.5 m. The sand transported offshore appears to have been supplied by the longshore sand transport toward the pier depression..

INTRODUCTION

A quantitative understanding of sediment transport processes on beaches is required for coastal sediment management, beach nourishment, and dredging of navigation channels. The US Army Corps of Engineers' Field Research Facility (FRF) at Duck, North Carolina produced valuable sediment transport data but the data analyses were mostly limited to longshore sediment transport (e.g., Miller 1999; Bayram et al. 2001). The depression under the FRF pier causes wave refraction and modifies the wave-induced circulation in the vicinity of the pier (Elgar et al. 2001; Johnson 2002). Furthermore, the pier pilings cause flow separation and energy dissipation. Nevertheless, the FRF pier provides a platform to measure the detailed cross-shore variations of suspended sediment transport during storms. The aim of this study is to analyze the FRF data and quantify the cross-shore and longshore sediment transport rates.

The velocities and sand concentrations measured along the FRF pier during the Sandy-Duck'97 experiment are analyzed here to examine the spatial and temporal variations of the current and suspended sand transport rate in the depression under the FRF pier. In the following, the velocity and sand concentration data for a storm in October 1997 are analyzed in detail. Previous studies addressed the wave field, circulation, concentration measurement and longshore sand transport (Elgar et al. 2001; Johnson 2002; Miller 1998). First,

---

[1] SIDMAR S.L., Avda. País Valenciano 22, Benissa, Alicante, 03720, SPAIN
[2] CACR, University of Delaware, Newark, DE, 19716, USA
[3] Kumamoto University, 2-39-1, Kumamoto JAPAN
[4] University of Cadiz, 11510 Puerto Real, SPAIN

the tide, waves, wind and bathymetry data during October 16–23, 1997 are presented. Second, the cross-shore and longshore velocities measured along the FRF pier are analyzed to examine the vertical, cross-shore and temporal variations of the mean and standard deviation of the measured velocities. Third, the measured sand concentrations are analyzed and coupled with the velocity data to estimate the cross-shore and longshore transport rates of suspended sand. The offshore suspended sand transport along the FRF pier is shown to be appreciable in comparison with a 100-year dune erosion event on the US Atlantic and Gulf Coast.

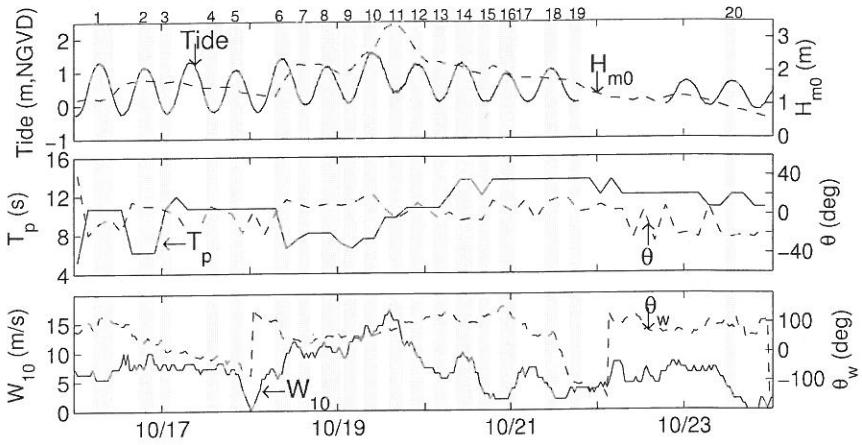

Figure 1. Storm tide, offshore significant wave height H_{m0}, spectral peak period T_p, predominant wave direction θ, wind speed W_{10} and direction θ_w during October 16–23, 1997.

FIELD DATA

The following field data are obtained from the FRF web site (www.frf.usace.army.mil) and personnel. Fig. 1 shows the water level measured by the tide gauge at the seaward end of the FRF pier during October 16-23, 1997. The FRF datum is the 1929 National Geodetic Vertical Datum (NGVD). The offshore significant wave height H_{mo}, spectral peak period T_p, and predominant wave angle θ were measured by the 240-m pressure gauge array in 8-m water depth for the duration of 8,192 s. The wave angle θ is zero for normally incident waves and positive counterclockwise. The wind speed W_{10} at 10 m above the water level and its direction θ_w are based on the anemometer data at the seaward end of the FRF pier. The wind direction θ_w is defined in the same way as the wave direction θ. The Sensor Insertion System (SIS) was deployed along the FRF pier within 1.5 hr of high or low tide during daylight hours (Miller 1999). The SIS is essentially a track-mounted crane without a lifting hook with

instrumentation mounted on the lower boom. The SIS can place instrumentation on the bottom in 9-m depth, 15 m away from the pier. Each of the 20 shaded columns in Fig. 1 indicates the duration of the SIS deployment along the FRF pier, which was referred to as a transect. Each transect included nine to eleven positions along the FRF pier.

Bathymetric surveys were conducted on September 16 and October 23, 1997. Fig. 2 shows the contours of 0, 2, 4, 6, and 8 m depths on these survey dates together with the pilings of the FRF pier. The piling diameter is 1 m. The cross-shore and longshore spacings of the pilings are 12 m and 5 m, respectively. The FRF cross-shore and longshore coordinates are positive offshore and northward, respectively. The incident wave angles for the 20 transects in Fig. 1 were within approximately 20 degrees mostly from the north of shore-normal. The wind angles for the 20 transects in Fig. 1 indicate that the wind exceeding 10 m/s blew roughly parallel to the shoreline from the north during the peak of the storm on October 19, 1997 when the significant wave height reached 3.5 m. The bathymetric change between the two survey dates was less than 0.6 m.

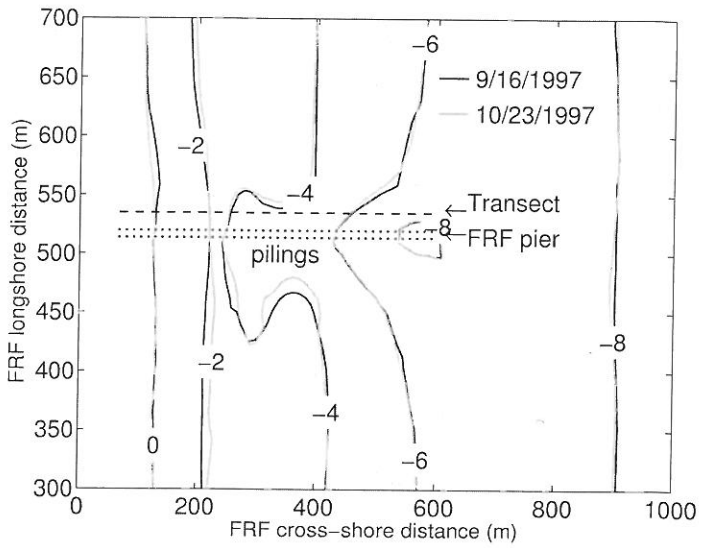

Figure 2. Depth contours measured on September 16 and October 23, 1997 in the vicinity of FRF pier where the pier is oriented 69.78 deg clockwise from true north and normal to the shoreline.

The beach profiles were measured at 41 m and 48 m north of the pier centerline on September 16 and October 23, 1997. The cross-shore coordinate x is taken to be positive landward with $x = 0$ in the 8-m depth where the offshore waves shown in Fig. 1 were measured. The vertical coordinate z is taken to be positive upwards with $z = 0$ at NGVD. The values of x at the seaward end of the

FRF pier and the mean shoreline are x_e =318 m and x_s = 789 m, respectively. The normalized onshore coordinate is defined as $x_* = (x - x_e)/(x_s - x_e)$ where $x_* = 0$ at $x = x_e$ and $x_* = 1$ at $x = x_s$.

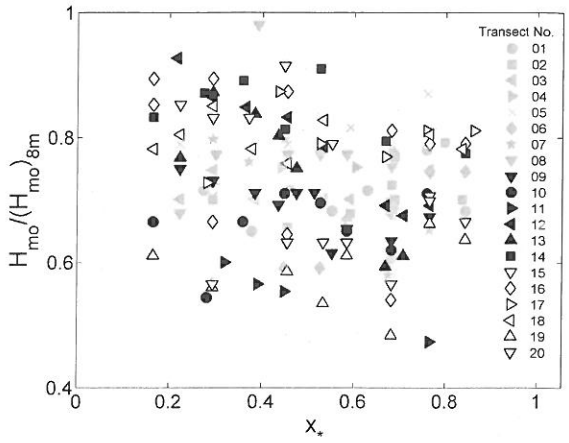

Figure 3. Significant wave height H_{mo} measured along pier normalized by offshore significant wave height for 20 transects.

The instrumentation frame attached to the SIS was held up drift on the north side of the pier during October 16–23, 1997. The instrumentation included a pressure gauge, electromagnetic current meters and optical backscatter sensors for sediment concentration measurements for the duration of 512 s with a sampling rate of 16 Hz (Miller 1999). An acoustic sonar measured the vertical distance to the local bottom at a sampling rate of 1 MHz. The mean water level was obtained from the measured mean pressure together with the assumption of hydrostatic pressure. The mean water depth h is the vertical distance between the mean water level and the local bottom.

The temporal variation of the measured pressure was converted to the wave-induced free surface variation using linear wave theory. The significant wave height H_{m0} is defined as $H_{m0} = 4s_\eta$ where s_η= standard deviation of the free surface variation. The measured values of H_{m0} for each transect are normalized by the value of H_{m0} in the 8-m depth shown in Fig. 1. The ratio $H_{m0}/(H_{m0})_{8m}$ was in the range of 0.5–0.9 as shown in Fig. 3 and varied little in the zone of $x_* =$ 0.2–0.8 except for transects 11 and 12 during the peak of the storm (see top panel of Fig. 1). The degree of irregular wave breaking at the position of the SIS was inferred by computing the fraction Q of breaking waves using the formula by Battjes and Stive (1985) and the hourly 10 min-averaged images taken from the camara C1 located at the 43-m high FRF observation tower. The estimated Q

is practically zero except for the most landward location near $x_* = 0.8$ where Q is less than 10%. Among a total of 82 daylight images, only 8 images (3 during the peak of the storm) suggested wave breaking. Consequently, the measurements have been conducted at the edge and seaward of the breaker zone.

CROSS-SHORE AND LONG-SHORE CURRENT VELOCITIES

The 512-s time series of the cross-shore velocity u and longshore velocity v measured at approximately 0.2, 0.4, 1.6 and 2.6 m above the local bottom are used to calculate the mean $\bar{u}$ and $\bar{v}$, which represent currents induced by waves, tide and wind, and the standard deviation s_u and s_v, which represent wave velocities in the 512-s record. The wave velocities are presented first because the analysis of s_u and s_v is simpler. The measured velocities are positive onshore and southward, respectively.

The measured standard deviations did not change much vertically and the vertically averaged values s_u and s_v are denoted as s_U and s_V which may be regarded as the standard deviations of the depth-averaged cross-shore and longshore velocities U and V, respectively. A linear regression analysis yields $s_V \sim 0.4\, s_U$ with a correlation coefficient of 0.65. If the predominant linear wave direction θ is estimated as $tan|\theta| = s_V/s_U$, the corresponding wave angle would be $|\theta| = 22°$ along the FRF pier. The measured s_U is compared with the standard deviation s_T of the depth-averaged wave velocity based on linear finite-depth wave theory (Kobayashi et al. 2008) where $s_T = C_p s_\eta / h$ with C_p = linear wave phase velocity based on the mean water depth h and the offshore period T_p. The measured values of s_U, s_η and h at the same location are used for the comparison which indicates that $s_U \sim 1.1 s_T$ as shown in Fig. 4. The local use of linear progressive wave theory is adequate for the estimation of s_U within an error of approximately 20%.

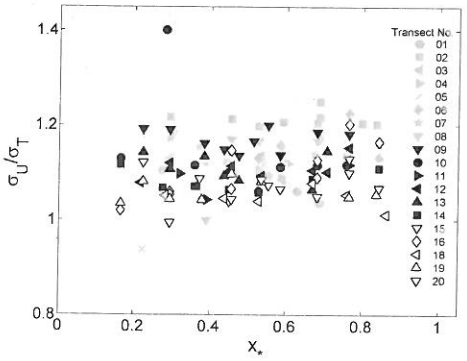

Figure 4. Standard deviation σ_U of cross-shore velocity measured along pier normalized by standard deviation σ_T of linear wave velocity for 20 transects.

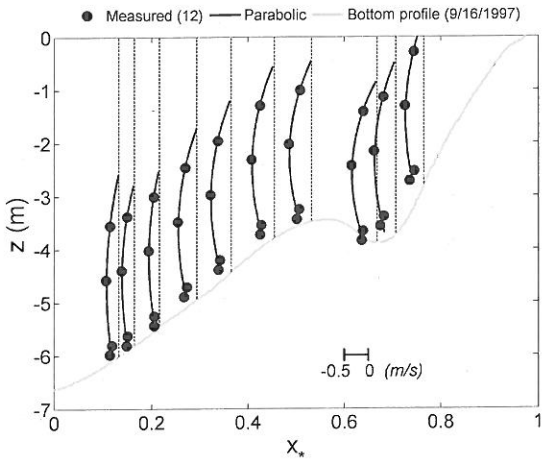

Figure 5. Offshore current $\overline{u}$ fitted to a parabolic profile at each cross-shore location for transect 12.

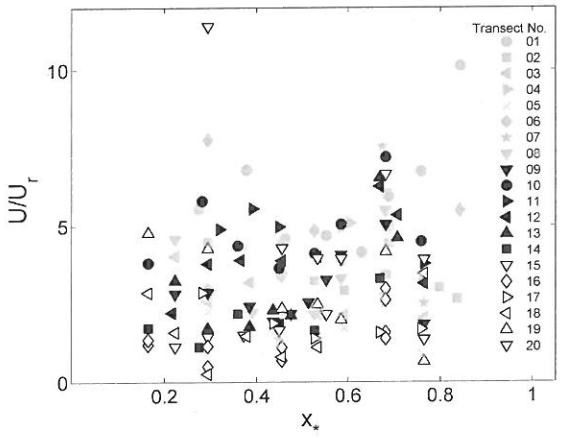

Figure 6. Vertically averaged offshore current $\overline{U}$ along pier normalized by return current U_r based on linear wave theory for 20 transects.

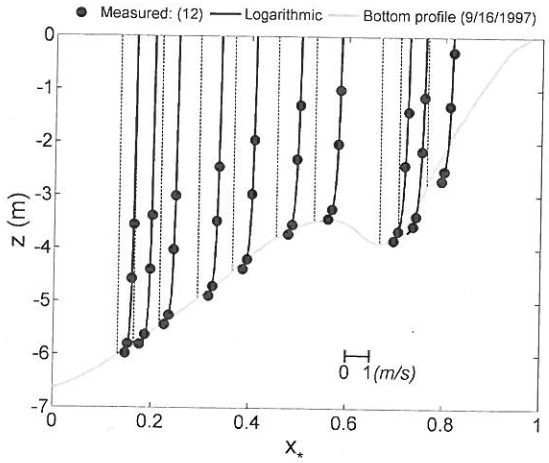

Figure 7. Longshore current $\overline{v}$ fitted to a logarithmic profile at each cross-shore location for transect 12.

The mean cross-shore current $\overline{u}$ was negative and offshore. The offshore current $\overline{u}$ is fitted to the parabolic profile given by $\overline{u} = (a_u z^2_m + b_u z_m + c_u)$ where z_m = elevation above the local bottom; and a_u, b_u and c_u = fitted coefficients for each parabolic profile. The offshore current $\overline{u}$ in the pier depression was of the order of 0.5 m/s during the peak of the storm. The fitted parabolic profile of $\overline{u}$ is integrated analytically in the region of $\overline{u} < 0$ between the bottom and the elevation of $\overline{u} = 0$ to obtain the vertically averaged offshore velocity $\overline{U}$ (Kobayashi et al. 2005). The measured offshore velocity $\overline{U}$ is compared with the return current U_r based on linear finite-depth wave theory under the assumption of alongshore uniformity (Kobayashi et al. 2008) where $U_r = (- g s_\eta s_t / C^2_p)$ where g = gravitational acceleration. The ratio $\overline{U}/U_r$ was as large as a factor 5 as shown in Fig. 6 when the offshore significant wave height H_{m0} in Fig. 1 was large and the measured offshore current $\overline{U}$ was strong. This implies that the strong offshore flow in the pier depression was fed laterally by the longshore current.

The longshore current $\overline{v}$ measured north of the pier was toward the south and the pier depression. The longshore current $\overline{v}$ is fitted to the logarithmic profile given by $\overline{v} = a_v ln(z_m/z_o)$ as shown in Fig. 7 where a_v and z_o = fitted

coefficients for each logarithmic profile. The longshore current in the pier depression was of the order of 1 m/s during the peak of the storm. The fitted logarithmic profile of $\bar{v}$ is integrated analytically from $z_m = z_o$ to $z_m = h$ to obtain the depth-averaged longshore current $\overline{V}$ as shown in Fig. 8. The measured $\overline{V}$ along each of the 20 transects has been compared with the longshore current model by Kobayashi et al. (2007) under the unrealistic assumption of alongshore uniformity. This model underpredicts the strong longshore current by a factor exceeding 2. This comparison suggests that the pier depression increases the longshore current updrift of the depression as expected from the relatively strong offshore current in the depression.

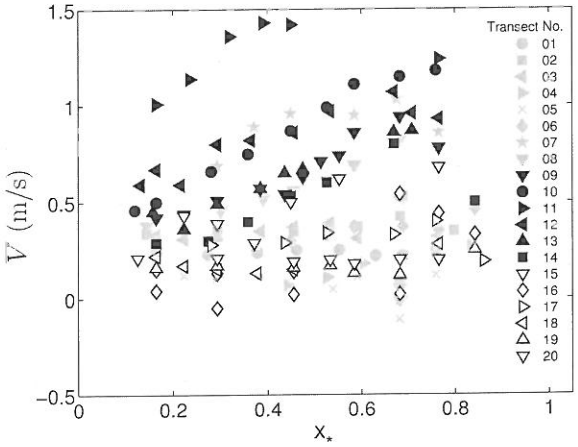

Figure 8. Depth-averaged longshore current $\overline{V}$ along pier for 20 transects.

SUSPENDED SEDIMENT TRANSPORT RATES

The sediment size on the beach at Duck decreases seaward. The median diameter is approximately 0.17 mm in the bar and trough region and 0.12 mm seaward of the bar (Miller 1999). Suspended sediment concentrations were measured using eight optical backscatter sensors (OBS) at eight elevations in the range of approximately 0.03–1.6 m above the local bottom. The bottom elevation measurement by the sonic altimeter may have an uncertainty of ±3 cm in the surf zone (Gallager et al. 1996). The 512-s record of the measured sand concentration c is analyzed in the following.

The mean concentration $\bar{c}$ is fitted to the power-law profile given by $\bar{c} = c_a(z_a/z_m)^m$ as shown in Fig. 9 where z_a = reference elevation above the local bottom which is taken as z_a = 3 cm corresponding to the lowest elevation of the

concentration measurement; and c_a and m = fitted coefficients for each power-law profile. It is noted that an exponential profile could not be fitted well for the present data. The suspended sand volume V_s per unit bottom area is obtained by integrating the fitted profile analytically from $z_m = z_a = 3$ cm to $z_m = h$. The measured V_s was in the range of 0.04–0.63 cm^3/cm^2 as shown in Fig. 10. The suspended sand volume remained large after the storm peak. It is noted that the degree of the fit for the power-law profile does not change much for $z_a = 3$, 5 and 10 cm. The uncertainty of the estimated suspended sediment volume per unit horizontal bottom area is less than 20%.

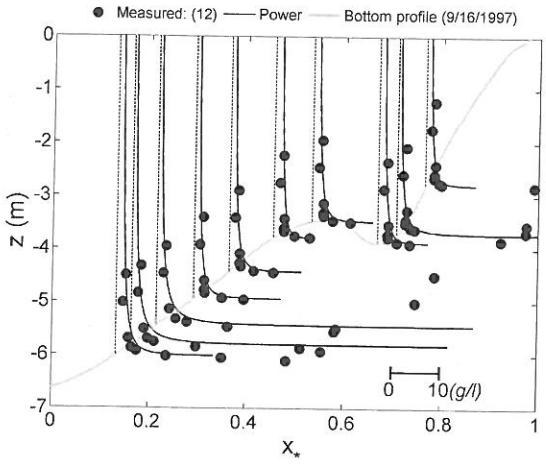

Figure 9. Mean concentration $\bar{c}$ of suspended sand fitted to a power-law profile at each cross-shore location for transect 12.

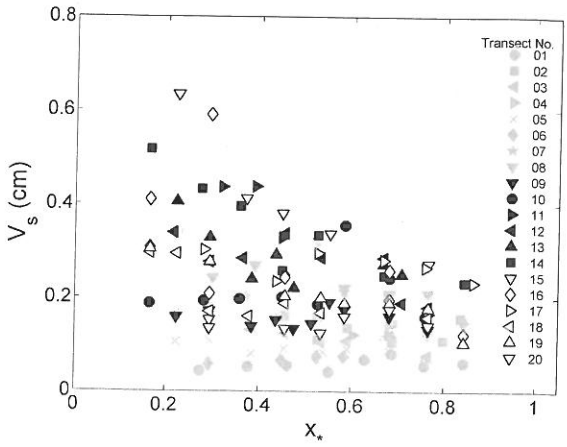

Figure 10. Suspended sand volume per unit area, V_s, along pier for 20 transects.

The 512-s records of c, u and v measured simultaneously are analyzed to obtain the time-averaged suspended sand transport rates expressed as

$$\overline{cu} = \overline{c}\,\overline{u} + \overline{(c-\overline{c})(u-\overline{u})} \tag{1}$$

$$\overline{cv} = \overline{c}\,\overline{v} + \overline{(c-\overline{c})(v-\overline{v})} \tag{2}$$

where the overbar indicates time averaging. The elevations of the concentration and velocity measurements were not matched exactly. The measured u and v at z_m~ 0.2, 0.4 and 1.6 m are paired with the measured c at the closest elevation. The three pairs do not yield a sufficient resolution for the vertical integration of $\overline{cu}$ and $\overline{cv}$. Consequently, an alternative approach is adopted to estimate the depth-integrated transport rates.

The terms $\overline{cu}$ and $\overline{c}\ \overline{u}$ in Eq. (1) are negative and indicate offshore suspended sand transport. The third term in Eq. (1) is positive and indicates onshore suspended sand transport due to the positive correlation of c and u (Kobayashi et al. 2005). Use is made of the relation of $\overline{cu} = 0.4\,\overline{c}\ \overline{u}$ although the correlation coefficient (CC) is 0.57 and relatively low. The depth-integrated offshore suspended sand transport rate q_{sx} is obtained by integrating $\overline{cu} = 0.4\,\overline{c}\ \overline{u}$ analytically from $z_m = z_a = 3$ cm to the upper limit of the region of $\overline{u} < 0$ where $\overline{u}$ and $\overline{c}$ are given by the fitted profiles. The concentration $\overline{c}$ above the region of $\overline{u} < 0$ was very small and neglected.

The terms $\overline{cv}$ and $\overline{c}\ \overline{v}$ in Eq. (2) are positive and indicate longshore suspended sand transport toward the pier depression. The third term in Eq. (2) is very small due to the negligible correlation between c and v. The depth-integrated longshore suspended sand transport rate q_{sy} is obtained by integrating $\overline{cv} = \overline{c}\ \overline{v}$ analytically from $z_m = z_a$ to $z_m = h$ using the fitted profiles of $\overline{c}$ and $\overline{v}$.

The depth-integrated offshore suspended sand transport rate q_{sx} is compared with the product of the average offshore current $\overline{U}$ and the suspended sand volume V_s per unit bottom area. The ratio $q_{sx}/\overline{U}\,V_s$ is plotted as a function of x_* for the 20 transects. The following simple formula was used by Kobayashi et al. (2008) to estimate the offshore suspended sand transport rate for the case of alongshore uniformity

$$q_{sx} = a\overline{U}V_s \tag{3}$$

where the empirical parameter a was 0.2, with an uncertainty of a factor of 2, for the small scale surf-zone experiments in a wave flume conducted by Kobayashi et al. (2005). The parameter a for the present field data is in the range of 0.1–0.4 outside the surf zone in the pier depression.

The depth-integrated longshore suspended sand transport rate q_{sy} is compared with $\overline{V}V_s$ where $\overline{V}$ is the depth-averaged longshore current. The ratio $q_{sy}/\overline{V}V_s$ is plotted as a function of x_* for the 20 transects. The following simple formula was used by Kobayashi et al. (2007) to estimate the longshore suspended sand transport rate mostly in the surf zone in the Large-scale Sediment Transport Facility at the US Army Engineer Research and Development Center

$$q_{sy} = \overline{V}V_s \tag{4}$$

Eq. (4) overpredicts q_{sy} slightly outside the surf zone in the pier depression. In short, Eqs. (3) and (4) may not be very accurate but allow one to estimate q_{sx} and q_{sy} using $\overline{U}$, $\overline{V}$ and V_s which may be predicted using horizontally two-dimensional nearshore wave, current and suspended sand transport models.

Finally, the offshore suspended sand transport rate q_{sx} per unit longshore length at the most seaward location (x_*~ 0.2) is plotted as a function of time for each of the 20 transects. The largest value of - q_{sx} is 3.5 m^3/hr/m for transect 11 at the peak of the storm. The temporal integration of - q_{sx} yields 130 m^3/m for the duration of 174 hours during October 16–23, 1997. This large sand volume must have been supplied mostly by the longshore sand transport toward the pier depression because the bathymetry did not change much as shown in Fig. 2.

CONCLUSIONS

Velocities and sand concentrations measured along 20 transects at the Field Research Facility (FRF) during October 16-23, 1997 are analyzed to examine the cross-shore and longshore suspended sand transport in the FRF pier depression. The depth-integrated offshore suspended sand transport rate q_{sx} is simply expressed as $q_{sx} = a\overline{U}V_s$ where $\overline{U}$ is the average offshore current, V_s is the suspended sand volume per unit bottom area, and the empirical parameter a is in the range of 0.1–0.4 in the pier depression. The onshore transport of suspended sand due to the correlation between the time-varying concentration and cross-shore velocity explains the reduction of a from unity. On the other hand, the correlation between the time-varying concentration and longshore velocity is negligible and the depth-integrated longshore suspended sand transport rate q_{sy} may simply be estimated as $q_{sy} = \overline{V}V_s$ where $\overline{V}$ is the depth-averaged longshore

current. These simple formulas are useful for morphological modeling using horizontally two-dimensional wave and circulation models.

The offshore suspended sand transport rate per unit longshore length at the end of the FRF pier is estimated to be as large as 3.5 m^3/hr/m. The sand volume transported offshore during October 16–23, 1997 is estimated to be 130 m^3/m and exceeds the dune erosion volume of 50 m^3/m for a 100-year event on the US Atlantic and Gulf coasts estimated by Hallermeier and Rhodes (1988). However, the corresponding bathymetric change was small, indicating the longshore sand supply toward the pier depression.

ACKNOWLEDGMENTS

This study was partially supported by the US Army Corps of Engineers under contract number W912BU-07-C-0013. The first author was supported initially by the Spanish postdoctoral scholarship MEC/FULBRIGHT and then by the postdoctoral fellowship program of the Centennial Anniversary Foundation of Kumamoto University, Japan. The authors would like thank Jarrell Smith, Chuck Long, Jane Smith and Bradley Johnson for providing the field data used in this study.

REFERNCES

Battjes, J.A., and Stive, M.J.F. (1985). "Calibration and verification of a dissipation model for random breaking waves." *J. Geophys. Res.*, 90(C5), 9159-9167.

Bayram, A., Larson, M., Miller, H.C., and Kraus, N.C. (2001). "Cross-shore distribution of longshore sediment transport: Comparison between predictive formulas and field measurements." *Coastal Eng.*, 44, 79-99.

Elgar, S., Guza, R.T., O'Reilly, W.C., Raubenheimer, B., and Herbers, T.H.C. (2001). "Wave energy and direction observed near a pier." *J. Waterway, Port, Coastal, Ocean Eng.*, 127(1), 2-6.

Gallagher, E.L., Boyd, W., Elgar, S., Guza, R.T. and Woodward B. (1996). "Performance of a sonar altimeter in the nearshore." *Marine Geology*, 133, 241-248.

Hallermeier, R.J., and Rhodes, P.E. (1988). "Generic treatment of dune erosion for 100-year event." *Proceedings of 21st International Conference on Coastal Engineering*, ASCE, 1197-1211.

Johnson, H.K. (2002). "Morphological modeling of the SandyDuck'97 experiment." *Proceedings of 28th International Conference on Coastal Engineering*, ASCE, 3370-3382.

Kobayashi, N., Agarwal, A., and Johnson, B.D. (2007). "Longshore current and sediment transport on beaches." *J. Waterway, Port, Coastal, Ocean Eng.*, 133(4), 296-304.

Kobayashi, N., Payo, A., and Schmied, L. (2008). "Cross-shore suspended sand and bedload transport on beaches." *J. Geophys. Res.*, 113, C07001, doi:10.1029/2007JC004203.

Kobayashi, N., Zhao, H., and Tega, Y. (2005). "Suspended sand transport in surf zones." *J. Geophys. Res.*, 110, C12009, doi:10.1029/2004JC002853.

Miller, H.C. (1998). "Comparison of storm longshore transport rates to predictions." *Proceedings of 26th International Conference on Coastal Engineering*, ASCE, 2954-2967.

Miller, H.C. (1999). "Field measurements of longshore sediment transport during storms." Coastal Eng., 36, 302-321.

KEYWORDS – ICCE 2008

PAPER TITLE: **SUSPENDED SEDIMENT TRANSPORT INSIDE AND OUTSIDE SURF ZONES**
Authors: **Andres Payo, Nobuhisa Kobayashi, Fumihiko Yamada, Juan J. Muñoz-Pérez**
Abstract number: **569**

Longshore sediment transport
Field measurements
Pier depression
Cross-shore sediment transport